Supporting Information:

Helical buckling of actin inside filopodia generates traction

N. Leijnse[†,$], L. B. Oddershede[†,$], & P.M. Bendix*[,†]

[$]Lundbeck Foundation Center Biomembranes in Nanomedicine, University of Copenhagen, 2100 Copenhagen, Denmark

[†]Niels Bohr Institute, University of Copenhagen, 2100 Copenhagen, Denmark

*Corresponding author: bendix@nbi.dk

Address: Niels Bohr Institute, University of Copenhagen,

Blegdamsvej 17, 2100 Copenhagen, Denmark

Mechanics of filopodia pulling

The mechanical behavior of filopodia is dictated by the material properties of the cell membrane including membrane tension, the membrane-cytoskeleton adhesion as well the mechanics of the filopodial actin. The holding force of a membrane tube which has been pulled from a cell is given by

$$f = 2\pi\sqrt{2\kappa_{\mathrm{mem}}(\sigma_o + W_o)}, \qquad [S1]$$

where κ_{mem} is the bending rigidity of the membrane and $\sigma_t = \sigma_o + W_o$ is the total membrane tension composed of the bound membrane tension σ_o and the additional tension W_o that arises from the membrane-cytoskeleton adhesion. The radius of the tube r_{tube} is determined from the bending rigidity and membrane tension

$$r_{\mathrm{tube}} = \sqrt{(\kappa_{\mathrm{mem}}/2\sigma_t)}\,. \qquad [S2]$$

The radius is affected by the extrusion velocity v_{pull} through the membrane tension in Eq. S2. Changes in pulling velocity leads to a transient change in σ_{t} and causes a change in tether radius. By having a cytosolic dye like calcein within the tube we can detect the changes in the tube radius by measuring the fluorescent signal during extrusion as shown in Fig. S13. The calcein signal scales with radius as $\sqrt{I_{\text{calcein}}} \propto r_{\text{tube}}$. A positive extrusion velocity leads to an increase in membrane tension and hence a decrease in radius (and decrease in fluorescence signal). Likewise a negative extrusion velocity (moving of the bead towards the cell) leads to a decrease in membrane tension and hence an increase in tube radius as shown by the increase in fluorescent signal in Fig. S13.

An effective viscosity, η_{eff}, arising from the membrane-cytoskeleton system results in an increase in the velocity dependent force on the trapped bead during extraction, as shown in Fig. S7A. This can be understood by isolating σ_{t} from Eq. S2 and inserting into Eq. S1 which gives the friction dependent force expressed as (1)

$$f = 2\pi\sqrt{2\kappa_{\text{mem}}\sigma_t} = \frac{2\pi\kappa_{\text{mem}}}{r_{\text{tube}}} \quad . \qquad \text{[S3]}$$

Hence, a dynamic increase in tension, during rapid extension, leads to a decrease in the diameter of the membrane tube and results in a dynamic increase in the force *f*, as shown in Fig. S7A.

The total membrane tension, however, contains a considerable contribution from the membrane-cytoskeleton adhesion. By disrupting the actin, using cytochalasin D or latrunculin B, we measure a significant drop in both the stationary as well as dynamic force as shown in Fig. S7B. This decrease results from the fact that W_{o} becomes close to zero in Eq. S1.

Buckling of the actin The energy of a filopodium held by the optical trap depends on the magnitude of the holding force *f*, delivered by the optical trap and the physical properties of the membrane and the actin shaft. Assuming a membrane tube with radius r_{tube}, membrane tension γ, and bending rigidity κ_{mem}, enclosing an actin shaft of contour length l, we obtain the energy by integrating the square of the curvature, $c=\left(\frac{\partial^2 \boldsymbol{r}}{\partial s^2}\right)$, along the contour parameterized by *s* (2, 3),

$$E = \frac{K_B T l_p}{2}\int_0^l \left(\frac{\partial^2 \boldsymbol{r}}{\partial s^2}\right)^2 ds + \left(\frac{\pi\kappa_{\text{mem}}}{r_{\text{tube}}} + 2\pi\gamma r_{\text{tube}} - f\right) L_{\text{tube}} \qquad \text{[S4]}$$

where l_p is the persistence length of the actin shaft, $K_\mathrm{B}T$ is the thermal energy and L_tube is the length of the membrane tube. The first term in Eq. S4 is the energy of bending of the actin shaft whereas the remaining energy terms relate to the bending and stretching of the membrane (4).

The actin shafts of filopodia typically formed localized helical buckles or exhibited a wavy character, as shown in Fig. 3A,E. We investigated if this could be caused by compressive helical buckling as theoretically predicted to occur in free filopodia due to the axial compressive load caused by the membrane tension (2, 3). The stability of a helical conformation can be tested by minimizing the energy given in Eq. S4. The outline of a helix with winding number n (helical windings per unit length) and radius R inside a tube of length L, can be mathematically described by

$$\boldsymbol{r}(s) = \begin{cases} x(s) \\ y(s) \\ z(s) \end{cases} = \begin{cases} R\cos(2\pi n s) \\ R\sin(2\pi n s) \\ s\sqrt{1-\pi^2 n^2 R^2} \end{cases}, \qquad \text{[S5]}$$

for a tube of length $L_\mathrm{tube} = l\sqrt{1-\pi^2 n^2 R^2}$. Eq. S5 has the shape of a helix as plotted inside the tube in Fig. 3F. Integration of Eq. S4 for a helix then gives the total energy of the membrane-actin system per unit contour length (3)

$$E/l = \frac{K_B T l_p}{2R^2}\left(1-\frac{L^2}{l^2}\right)^2 + \left(\frac{\pi\kappa}{R} + 2\pi\gamma R - f\right)L/l \qquad \text{[S6]}$$

and is plotted in Fig. S9. There exists an energy minimum for a relative shortening of $L/l \approx 0.95$ for a tube with $R \approx 95$ nm. However, after adding the external force needed to hold a pure membrane tube of $f = 2\pi\sqrt{2\kappa_{mem}\sigma} \approx 8\,\mathrm{pN}$ no energy minimum is obtained (see Fig. S9*B*). Although we often measured a transient decrease in the force as shown in Fig. S6, the measured holding forces were typically much higher than 8 pN. Therefore we exclude the possibility that the helical buckles, are caused solely by axial compressive load by the membrane. This could still be relevant for free cellular filopodia but in our experiments the optical trap diminishes the axial load on the actin and hence compressive buckling cannot occur.

Drag of a cylinder in a membrane The correction factor $\alpha_{\perp}$ in Eq. 2 in the manuscript depends on the length to thickness ratio, $p = L/2R_{\mathrm{prot}}$, of the cylindrical rod. The subscript means that we consider the drag orthogonal to the cylindrical rod. The drag from a single cylinder moving at a constant speed through the membrane is (5, 6):

$$F_{\mathrm{drag}} = \frac{4\pi\eta_{\mathrm{mem}}L}{\ln\left(\frac{L}{2R_{\mathrm{prot}}}\right)+\alpha_{\perp}} \quad , \qquad \text{[S7]}$$

where η_{mem} is the membrane viscosity, L is the length of the transmembrane cylinder, R_{prot} is the radius of the protein, and $\alpha_{\perp}$ is a correction factor which depends on the ratio $p = L/2R_{\mathrm{prot}}$ and the subscript denotes that we are considering the transverse drag on the cylinder. Tabulated values exist for $\alpha_{\perp}$ (5) and these can be interpolated by the function $\alpha_{\perp}(p) = 0.84 + 0.19/p + 0.23/p^2$ (7). Using $R_{\mathrm{prot}} = 0.64$ nm (8) and L = 5 nm (approximate thickness of membrane) we get $\alpha_{\perp} = 0.90$.

The total torque around the axis of the shaft therefore becomes

$$\tau_{\mathrm{N}} = r_{\mathrm{tube}}N_{\mathrm{anchors}}F_{\mathrm{drag}} = r_{\mathrm{tube}}N_{\mathrm{anchors}}\frac{4\pi\eta_{\mathrm{mem}}L}{\ln\left(\frac{L}{2R_{\mathrm{prot}}}\right)+\alpha_{\perp}}. \qquad \text{[S8]}$$

Image analysis

The location of a coil was found by summing the pixel intensities from the actin orthogonal to the filopodium after subtracting off the background intensity. Each image was therefore represented by a vector at a given time point and bending of the actin appeared as an intensity peak. Kymographs were obtained by constructing a matrix from these vectors in which every row represents a given time point. Importantly, to obtain the correct location of the coil relative to the tip of the filopodium, we performed parallel tracking of the centroid intensity from the bead which allowed us to correct for any movement of the trapped bead and possible axial shortening could thus be detected within the actin shaft. Velocities of the coils were quantified as the slope in of the trajectories that appeared in the kymographs (see Fig. 2D). Rather than quantifying the

average velocity, we resolved the local velocities as a function of distance relative to the cell body by calculating the local gradient along the curve resulting in data as presented in Fig. 2G.

Curvatures of the actin along the filopodium were quantified by fitting a Gaussian function to the intensity distribution for every pixel line orthogonal to the filopodium. The interpolated center position of the Gaussian fit yields a sub-pixel resolution estimate for the location of the filopodium. The resulting center positions for all orthogonal pixel lines constitute the skeleton of the filopodium as shown by the solid lines in the insets of Fig. 4C. The curvature along the filopodial skeleton is calculated using the expression

$$c(x) = \frac{|y''(x)|}{(1+(y'(x))^2)^{3/2}} \quad , \qquad [S9]$$

where y is the position along the orthogonal direction and x is along the filopodium. $y'(x)$ and $y''(x)$ denote the spatial derivatives with respect to x.

Investigation of the correlation between the force and the presence of the actin at specific positions within the filopodium was carried out by finding areas of intensity falling above a threshold defined by threshold = $\langle I \rangle_{bg} + \sigma_{bg}$, where $\langle I \rangle_{bg}$ is the average intensity in a background region of interest and σ_{bg} is the standard deviation of the intensities from the same region of interest. Only connected clusters of pixels were quantified to filter out single pixel noise. By selecting regions of interests along the filopodium, we tested for correlation between the measured force (resulting in a displacement of the trapped bead) and the actin signal which were acquired simultaneously. An example of the analysis is shown in Fig. S11 and in Supplementary Movie 5.

Three dimensional rendering Three dimensional (3D) images of filopodia during retraction of the actin were obtained from confocal images taken at different heights. Images were deblurred in ImageJ (9) using the Richards-Wolf model Point Spread Function for deconvolution. A 3D volume viewer in ImageJ was used to reconstruct the deblurred images into 3D images as shown in Fig. 1A,B and Movie 1.

Coil velocities Kymographs were analysed using Image Processing Toolbox in Matlab (10). Intensity edges were detected using the *canny* method within the built-in Matlab *edge.m* function which detects local maxima of the intensity gradients in an image. The resulting binary image (BW) was area-filtered using the Matlab function *bwareaopen.m* to remove edges resulting from image noise. Finally, the edges of interest were identified and selected using the Matlab function *bwselect.m*. The coordinates (*x,y*) were located using the *find.m* function, ([*x,y*] = *find*(BW == 1)), and subsequently the velocities were obtained by calculating the corresponding spatial gradients of the connected pixels within the image. To ensure that coil displacements were within the reference frame of the trapped bead, the position of the coil was corrected with any displacement of the trapped bead. The bead was tracked using centroid tracking (of the intensity distribution) of the signal from the light reflected by the bead.

Actin and force correlation The actin intensity near the tip was obtained by selecting a Region Of Interest (ROI_{tip}) containing the filopodial tip. The intensity within the ROI_{tip} was quantified by summing all intensities above the background threshold which was obtained from another ROI_{bg} (mean + standard deviation of the pixel values) containing a background area outside the cell. The actual quantification relied on first making the area within ROI_{tip} binary with all pixels below the background threshold being '0' and all pixels above the threshold being '1'. Single pixel noise was filtered out using *bwareaopen.m*. The binary image was multiplied, pixel-by-pixel, with the raw image and finally all the elements in the resulting matrix were summed to give the total actin signal. The corresponding displacement (and consequently the force) of the trapped bead was calculated using centroid tracking of the trapped bead (in the reflection channel) or by using the signal from the quadrant photodiode.

Actin curvatures Curvatures along the actin shaft were analyzed using Matlab by tracking the skeleton of the actin shaft. The size of the buckles presented in Fig. S1 was found by integrating the area under the curve by tracing the skeleton of the actin shaft. Before integration the images were rotated such that the filopodium was aligned with the *x*-axis of the image.

Experimental setup

The setup consisted of an optical trap with a quadrant photodiode detection system integrated in a confocal laser scanning microscope. The setup allows optical trapping and measurements of forces exerted on the bead simultaneous with confocal imaging of fluorescent signals. The optical trap consisted of a Nd:YVO4 (5 W Spectra Physics BL106C, TEM_{00}, λ=1064 nm) laser implemented in an inverted Leica confocal microscope (TCS SP5). The laser was focused through a high numerical aperture water immersion objective (Leica 63 x, 1.2 NA, apochromatic water (No. 11506279)) to a diffraction limited spot inside the sample chamber. A three dimensional piezoelectric stage (PI 731.20, Physik Instrumente, Germany) allowed positioning of the sample relative to the laser focus with nanometer precision. The scattered laser light passing the sample was collected by a condenser (Leica, P1 1.40 oil S1) and focused onto a quadrant photodiode (S5981, Hamamatsu). Optical trapping data was acquired by a data acquisition card (NI PCI-6040E) at a sampling frequency of 1 kHz and processed by custom written LabVIEW programs (LabVIEW 2010, National Instruments). For simultaneous force measurements and confocal imaging, a bead inside the chamber, visualized in bright field mode, was optically trapped and a high frequency time series (22 kHz) of its positions was acquired in order to calculate the trap stiffness via power spectral analysis using a Matlab program (11). The fluorescent GFP-Utrophin (excited at λ_{ex}=488 nm) and the reflection signal (λ_{refl}=458 nm laser) from the cell and the trapped bead (after optimizing the image acquisition settings) were recorded using Leica's LAS AF software. The trapped bead was brought into contact with a HEK cell for less than one second and pulled back to form a contact with a filopodium either by translating the stage manually or via a LabVIEW program with a controlled velocity. A telescope lens in the beam path of the optical trap allowed adjustment of the trap focus with respect to the microscope focus in order to align the tether with

the imaging plane. A pinhole of 1 airy unit was used in the confocal imaging to reject out of focus light.

Cell and sample preparation

F-actin labeling Cells cultured in T25 flasks (90% confluent) were transfected to express GFP-Utrophin, a live cell reporter for F-actin (12), using Effectene transfection reagent (Quiagen) according to the manufacturer's protocol and 0.6-1 µg/µl plasmid. While the effectene-plasmid mix was prepared, the cells washed with DPBS and detached from the bottle using with 0.5 ml TrypLE Express. They were re-suspended in 5 mL warm growth medium and centrifuged at 1000 rpm for 5 mins. The supernatant was removed and the cells were re-suspended in 4ml fresh growth medium. 1ml of cell suspension together with 2 ml of fresh growth medium were added to one well of a 6-well plate (Nunclon Δ Surface, Nunc). The effectene-plasmid mix was added and the cells were left in the incubator for 4 hrs before the medium was carefully exchanged with fresh warm growth medium. The cells were used for measurements 1-2 days after transfection.

We tested the effect of transfection and fluorescent excitation of GFP-Utrophin by measuring the holding force of a filopodium in cells that were transfected with GFP-Utrophin and not transfected, respectively, over time a course of 500 s. We measured similar force dynamics for transfected and not transfected cells as shown in Fig. S6*A* as well as for cells transfected with Lifeact-GFP (Ibidi) (13) which was used to transfect the cell in used in Fig. 4B,C. Similarly, the fluorescent excitation did not alter the force dynamics of the transfected cells as shown in Fig. S6.

Sample preparation For photodiode force detection measurements we used thin closed chambers made from two clean coverslips (24x50 mm #1.5 and 18x18 mm #1, both, Menzel-Gläser). For experiments where the bead movement was calculated from image analysis (centroid tracking), the cells were seeded in MatTek glass bottom dishes. HEK cells transfected to express GFP-Utrophin were detached from a 6-well, suspended in warm growth medium, and were poured into a petri dish containing 2 clean coverslips (24x50 mm #1.5) or into 4 MatTek dishes. The samples were left in the incubator (typically for 2-6 h) in order to allow the cells to adhere to the coverslips (while still having rounded shape). The density of cells was chosen such that most cells were

isolated. A coverslip with attached cells was taken out of the petri dish and a perfusion chamber was created by adding two stripes of vacuum grease on this coverslip and placing a clean coverslip (18x18 mm, #1, Menzel-Gläser) on top. The chamber was filled with Dulbecco's PBS (DPBS) (1X, [+] $CaCl_2$, [+] $MgCl_2$, Gibco), which was used as imaging medium, containing *d* = 4.95 µm streptavidin coated polystyrene beads (Bangs Laboratories) and sealed off with vacuum grease. The experiments were conducted at room temperature and the chambers were used for ~2.5 h after being prepared.

Cytoplasmic labeling The cells were cultured and closed chambers were prepared as described above. Before sealing the chamber it was flushed once with DPBS and then incubated for 1 min with 250 µL (DPBS):1 µL (Calcein AM (Invitrogen)) and preparation continued as described above.

Cytochalasin D and and Latruculin B treatment The cells were cultured, transfected to express GPF-Utrophin, and the chambers were prepared as described above. Before sealing the chamber, 5 µM cytochalasin D (Sigma, stock solution in DMSO) or 1 µM latruculin B (Sigma, stock solution in DMSO) in DPBS was added to the chamber together with *d* = 4.95 µm streptavidin coated polystyrene beads and sealed off with vacuum grease. The chamber was left to incubate at room temperature for 30 min (cytochalasin D) or 1 h (latrunculin B) before conducting experiments.

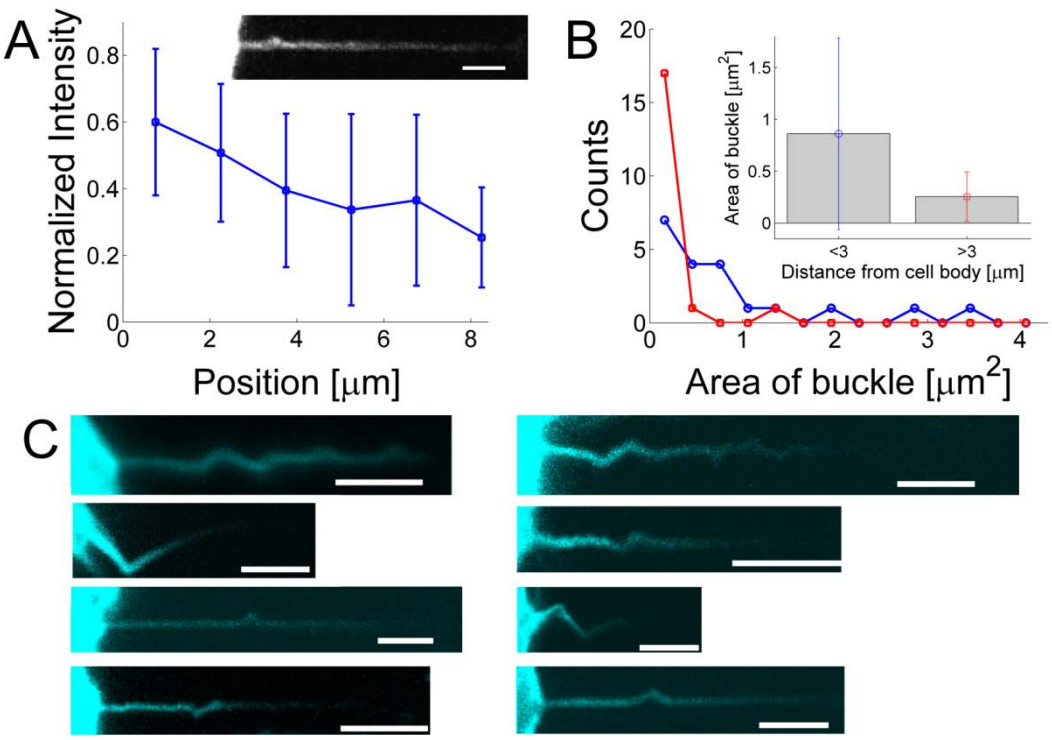

Figure S1 | Size of the actin buckles correlates with the thickness of the actin shaft and hence the proximity to the cell body. (A) Normalized average intensity of 17 actin shafts that were in focus just prior to buckling. The quantification reveals that the intensity decreases as a function of the distance to the cell body. Since the actin fluorescence scales with the number of F-actin filaments this shows that the actin shafts are, on average, thicker near the cell body. Image shows an example of a typical shaft before buckling, scale bar is 2 µm. (B) Quantification of the projected area under single buckles shows that buckles have a larger extent when the buckle is located within 3 µm from the cell body (blue circles) than when the buckle is located further away than 3 µm from the cell body (red squares). Inset shows the mean area of buckles in the two distance regimes. The total number of buckles analyzed was N = 34. (C) Typical images of buckles at different distances from the cell body. The top left image is from the same experiment as in Fig. 1B in the manuscript. Scale bars 3 µm.

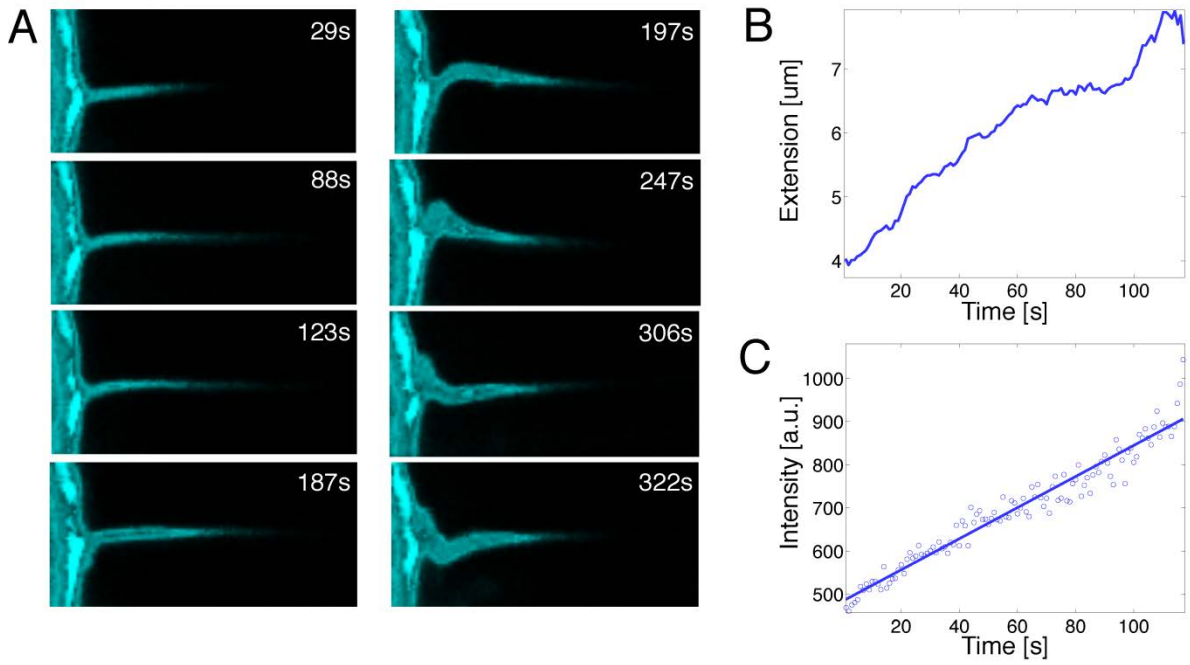

Figure S2 | Kinetics of F-actin in a filopodial membrane tube at various time points (t = 0 corresponds to tether formation). (A) Images of actin polymerizing into the membrane tube followed by bending of the actin shaft after ca. 200 s. (B) Quantification of the extension of the F-actin shaft into the tube versus time. (C) Total intensity of the actin inside the filopodium versus time.

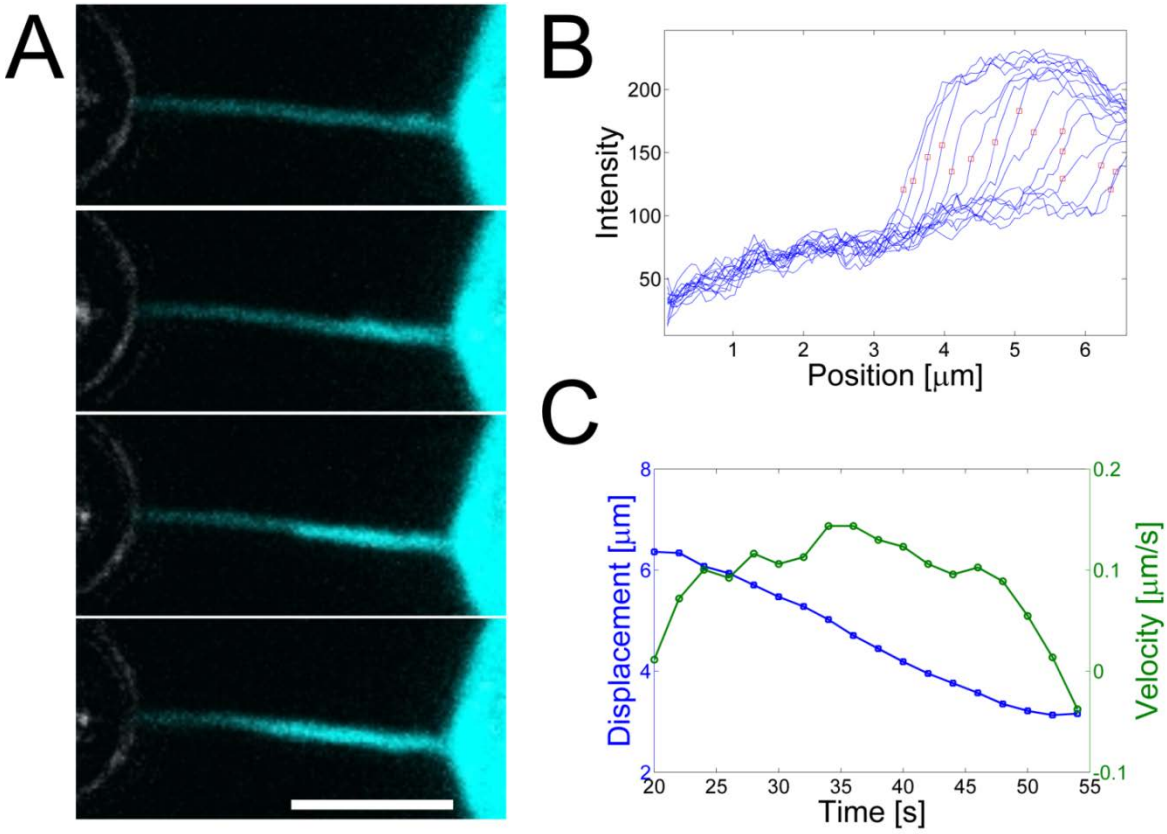

Figure S3 | Actin polymerization velocity into a membrane tube. (A) Images showing how the actin intensity increases from the cell body (right) towards the trapped bead (left). Scale bar, 3 μm. (B) Intensity profiles along the actin shaft at a few different time points. Initially, the intensity along the shaft exhibits a high gradient near the cell body. The location of this high gradient region subsequently moves away from the cell body with time. The red squares denote the maximum in gradient of the respective curves. (C) The displacement and velocity of the red squares in (B) as a function of time. The curves in (C) are smoothed with a running average of 5 time points.

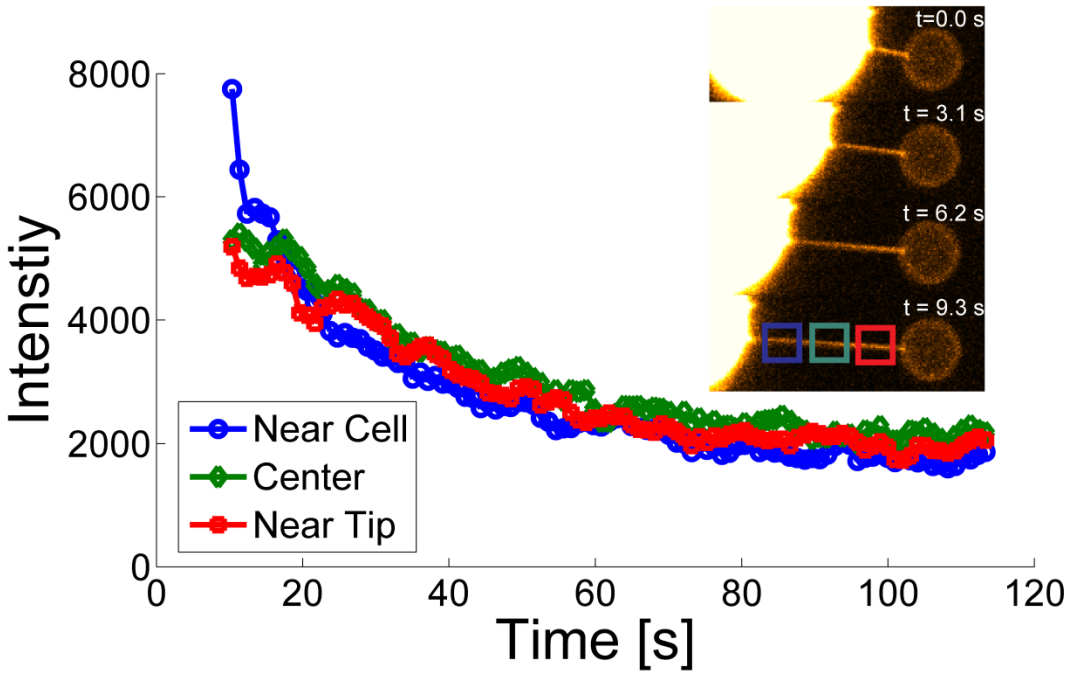

Figure S4 | Kinetics of calcein diffusion within the pulled tube. Unlike GFP-Utrophin, calcein AM fills the tube immediately during pulling and subsequently only bleaching is detected. Images show a typical example of the intensity of calcein during pulling. After pulling the tube with 1 µm/s for 10 s, the pulling speed is set to 0.05 µm/s after which the intensity is recorded within the blue, green and red squares for 100 s. The graph shows the quantification of the intensity over time for the three respective regions on the tube and the similar bleaching rates confirm that diffusive mixing is fast.

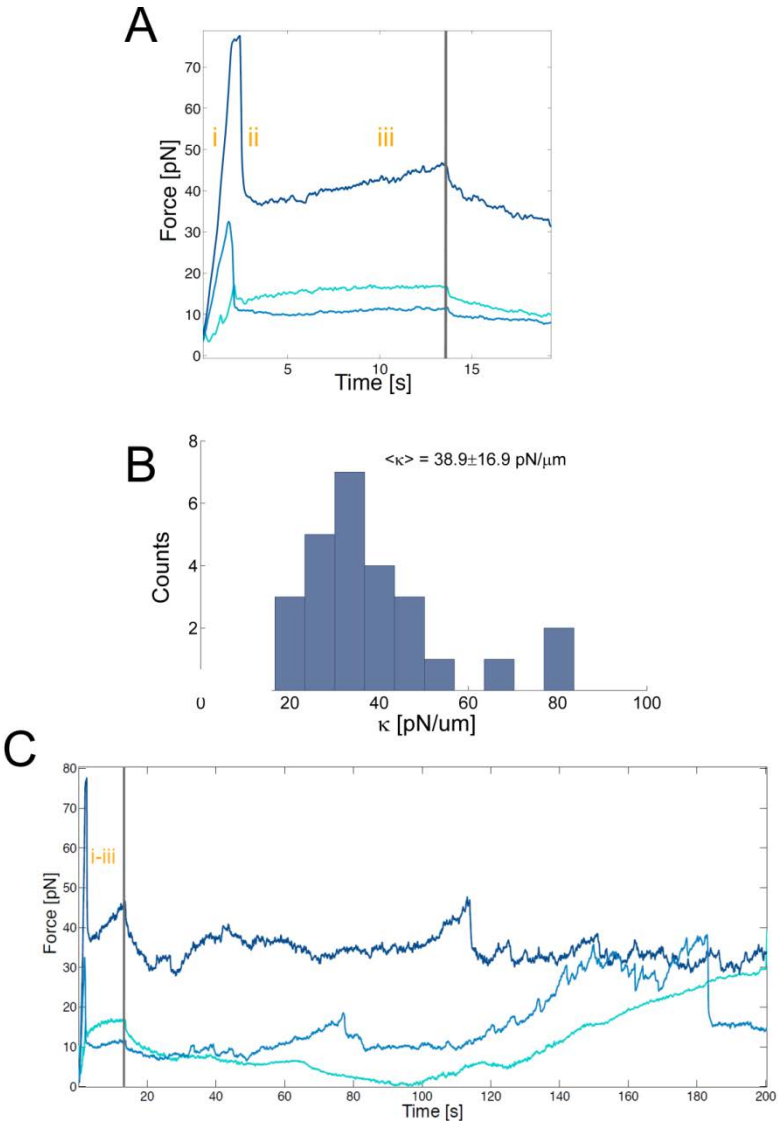

Figure S5 | Force behavior during elongation and long term holding of a filopodium. (A) Force curves for three different filopodia elongations using v_{pull} = 1 µm/s for 13 s. Initially, (i) the force rises linearly, reflecting the Hookean behavior of the cytoskeleton that is deformed before a tether is pulled away from the cell. (ii) Subsequently, a sudden decrease in force occurs upon cytoskeleton detachment from the plasma membrane (iii) and is followed by a nearly flat plateau as a filopodium is extracted. As the extraction velocity is set to zero (at t =13 s) the viscoelastic filopodium/actin system relaxes exponentially to a lower plateau. (B) Statistics of the initial slopes (i) as shown in (a) which equal the spring constant κ of the elastic response of

the cytoskeleton to filopodial extension. (C) Force dynamics of entire experiment in (A) lasting 200 s. The initial pulling velocity was v_{pull} = 1 µm/s and was set to zero after 13 seconds.

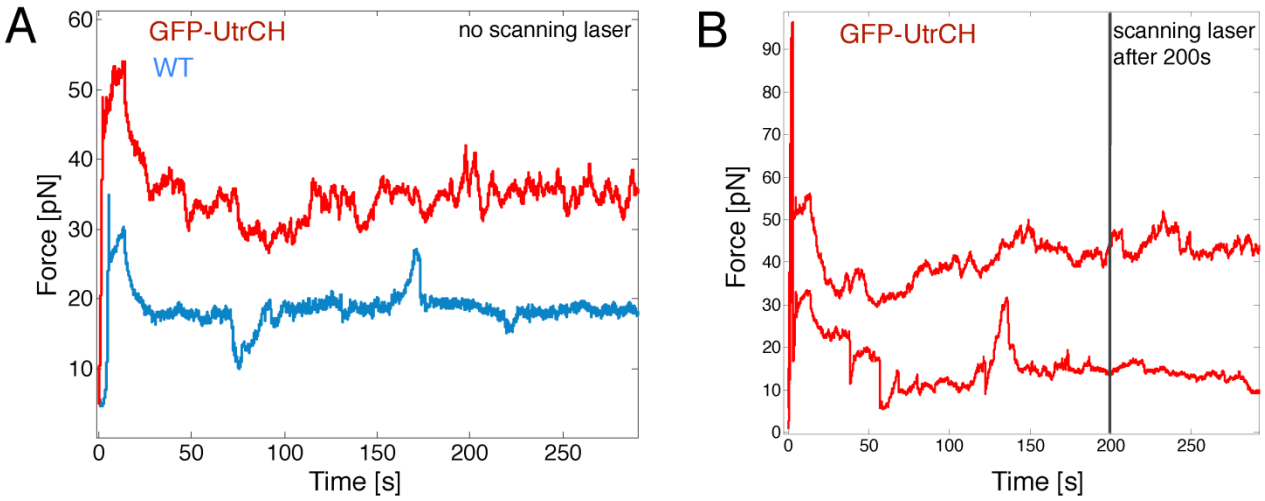

Figure S6 | Effect of the confocal scanning laser, for imaging the actin, on the force dynamics of membrane tethers held by an optical trap for ca. 300 s. (A) The force recorded in absence of the scanning laser in wild type (blue curve) and in GPP-Utrophin expressing HEK cells (red curve). (B) Two different examples of the force recorded before and after the scanning laser was turned on after 200 s in GFP-Utrophin expressing HEK cells.

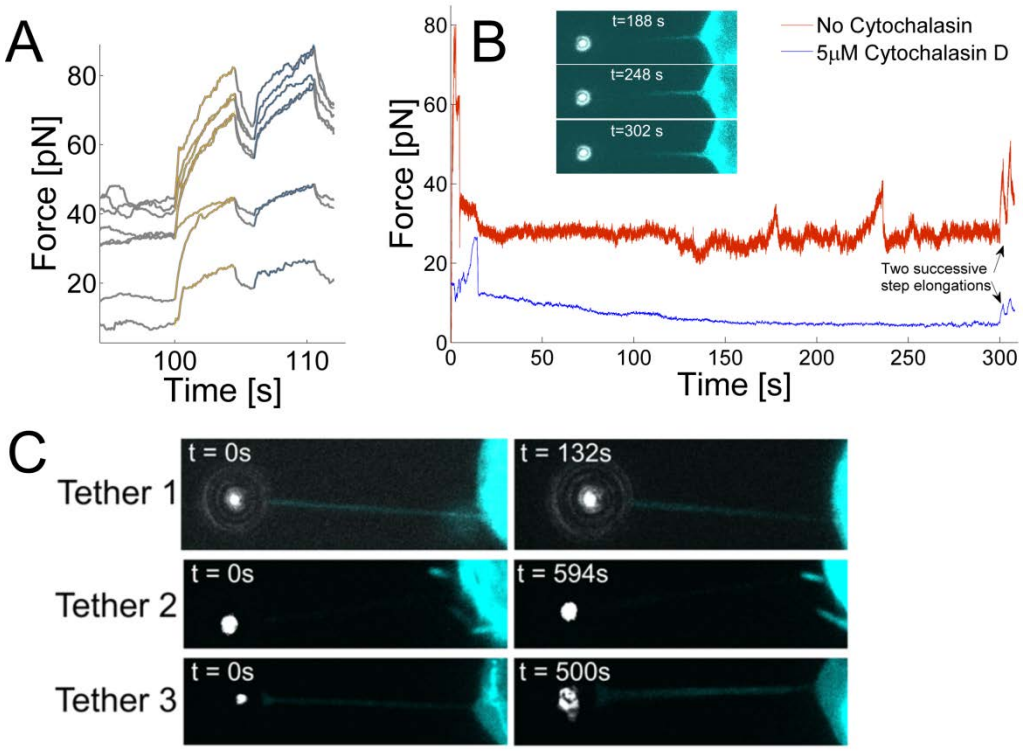

Figure S7 | Actin-membrane friction during step pulling. (A) Slow pulling at v_{pull} = 0.05 µm/s followed by two consecutive fast pulls with v_{pull} = 1 µm/s leads to an increase in the force to a higher plateau value due to viscous friction of the combined actin and membrane system. The force asymptotically approaches $F(t) = F_\infty - (F_\infty - F_1)*\exp(-(t-t_1)/ \tau))$ where F_1 is the initial force and τ = 1.7 ±0.4s (N = 8, first pull) and τ = 2.3 ±0.7s (N=8, second pull). Upon termination of the pulling (v_{pull} = 0) the force relaxes again towards a lower plateau value in a dissipative manner. (B) The frictional effect of the actin cytoskeleton is observed by disrupting the actin using cytochalasin D. The rapid elongation at the end of the time series (v_{pull} = 1 µm/s) after the filopodium has been held constant for around 285 s produces a significantly lower increase in the force when the actin is disrupted (blue curve) compared to when the F-actin is still present (red curve) thus showing the large contribution from the actin-membrane friction. Inset images show that the actin signal is still present but no dynamics is observed. (C) Disruption of actin using latrunculin B. Three tethers are pulled and subsequently the GFP-Utrophin signal is recorded every 2 s. No actin or force dynamics was observed in such tethers. The remaining stationary and uniformly fluorescent signal stems from GFP-Utrophin in the cytosol. Some

filopodia were still visible as in the middle right image and these were also stationary for the 594 s of acquisition. The three tethers have a length of ~15, ~10 and ~20 µm.

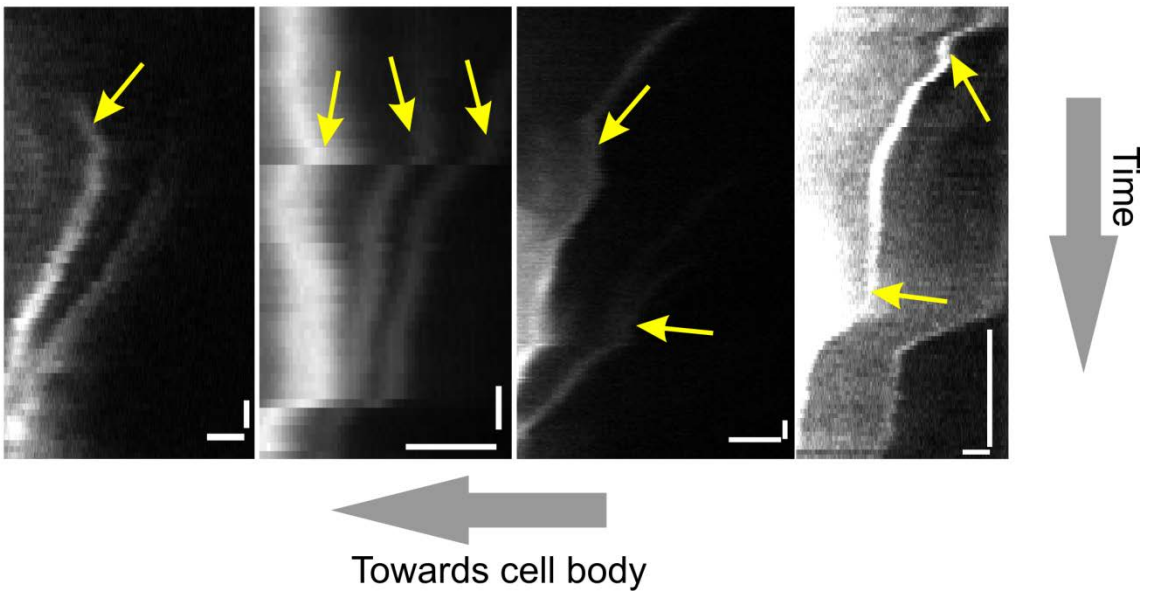

Figure S8 | Examples of coil velocities that occurred simultaneously with an increase in force on the optically trapped bead. The yellow arrows point at events where the coil velocity either reversed sign (travelled away from the cell body as in Fig. 2B in the manuscript) or nearly became zero. Scale bars in all images correspond to 1 µm (horizontal) and 10 s (vertical).

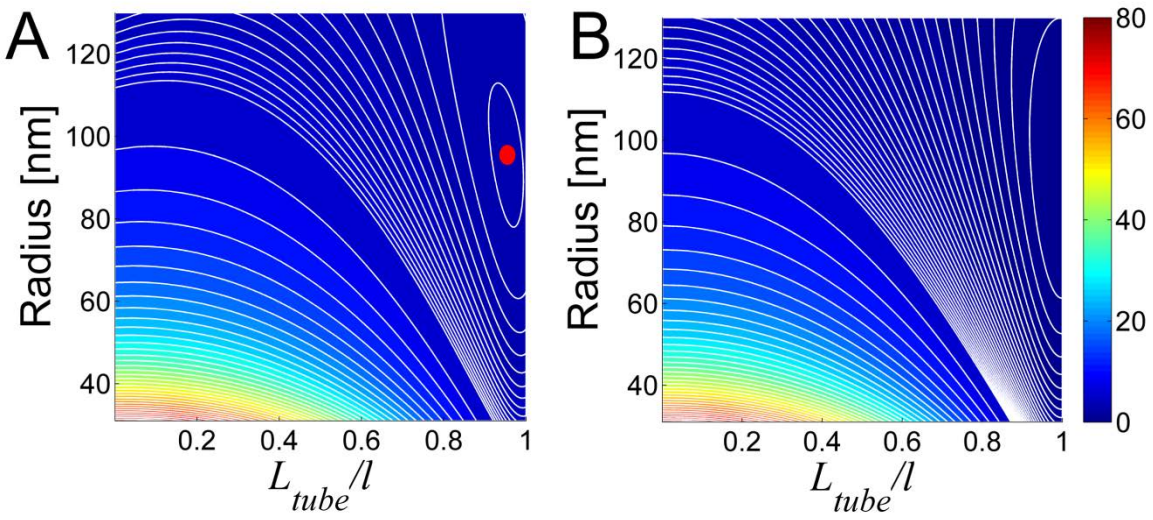

Figure S9 Calculations of the energy of a system consisting of an actin bundle (10 not cross-linked filaments) of contour length l = 10 µm inside a membrane tube of Radius r_{tube}, and tube length L_{tube}, see Eq. S4 and Eq. S6. (A) The plot shows the energy without an optical trapping force applied to the tip. The system has an energy minimum when $r_{\mathrm{tube}} \approx$ 90 nm (red circle) and at a relative shortening of $L_{\mathrm{tube}}/l \approx$ 0.95. (B) When an optical trap is used to hold the membrane tube (holding force 8 pN), the energy minimum disappears, and hence no compressive helical buckling takes place, in contrast to experimental observations. The colorbar is in units of $K_{\mathrm{B}}T$ /nm.

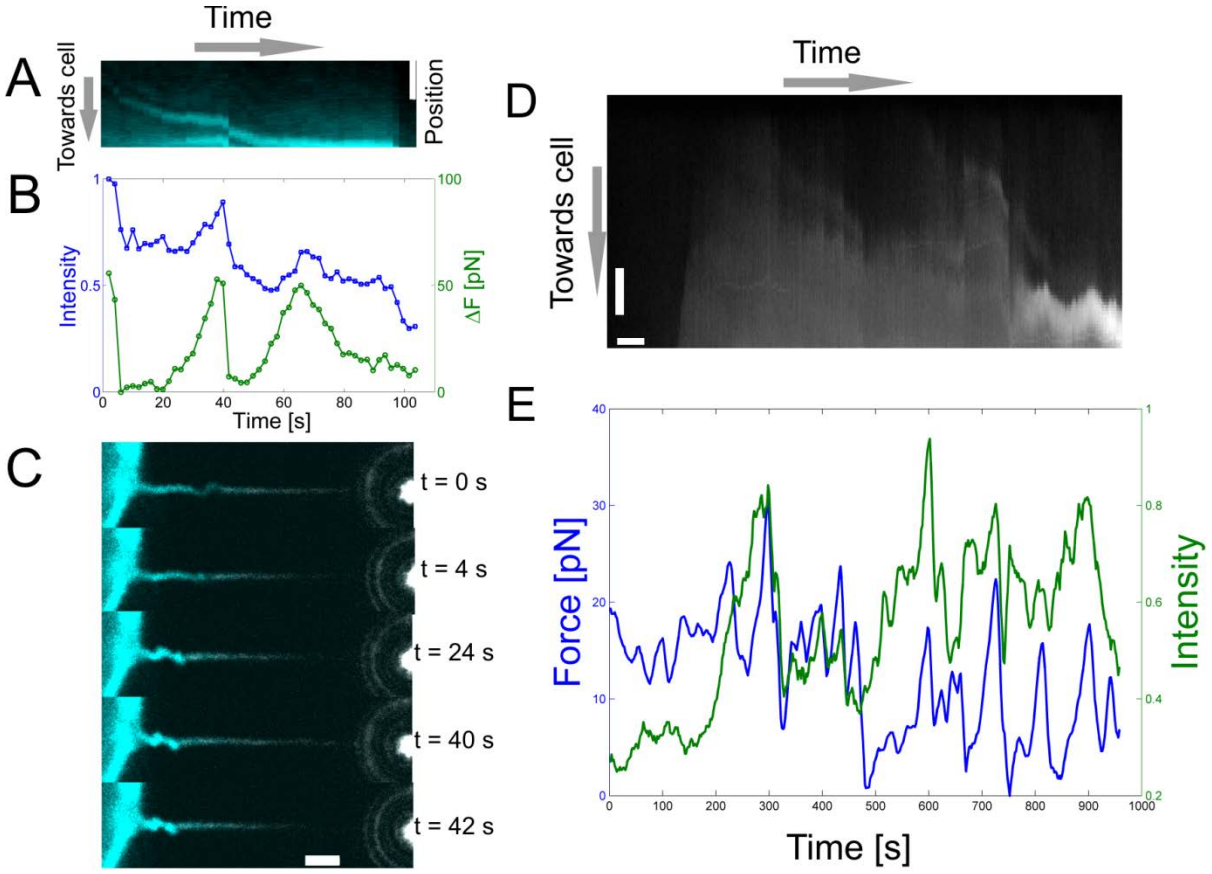

Figure S10 | Correlation between the presence of actin at the tip and a displacement of the trapped bead towards the cell body (pulling). (A) Kymograph showing the position of helical bends on the actin shaft versus time. An abrupt change in velocity is detected at ~41 s. Scale bar, 2 µm. (B) Simultaneous recording and quantification of the pulling force and actin signal recorded near the tip as a function of time. After ~41 s the actin content (blue curve) decreases abruptly simultaneously with the force (green curve). (C) Snap shots of the data from (A,B) reveal that the actin shaft is bending locally and traveling backwards. Even during significant pulling (t = 40 s) the actin shaft is observed to bend locally thus excluding the possibility of compressive buckling. The images are formed by an overlay of the actin (cyan) and reflection signal from the bead (white). Scale bar, 2 µm. (D) Kymograph of another experiment showing several buckles moving along the filopodium. After ~100s the actin polymerized into the membrane tube which is detected as an edge in the kymograph with positive slope. Subsequently, several buckles appeared which are detected as high intensity gradients in the kymograph. Scale bar, 2 µm and 10 s. (E) Simultaneous detection of the intensity of actin (2 µm

tip region) and the corresponding force on the trapped bead. The bead displacements in this figure were detected using image analyzes and not the photodiode detection system.

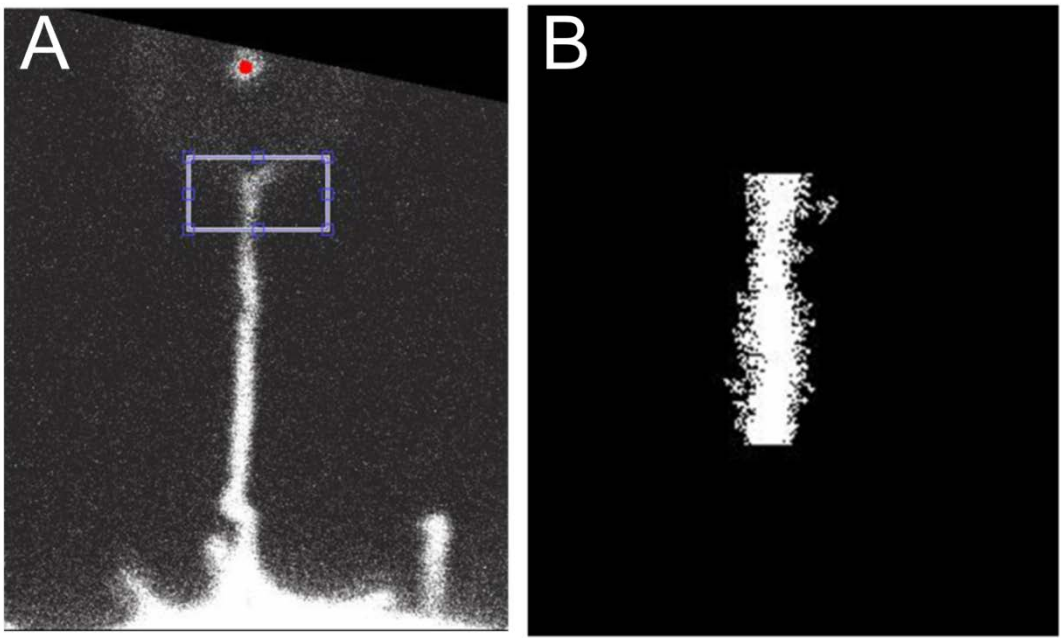

Figure S11 | Quantification of actin at the filopodial tip. (A) A Region Of Interest (ROI) is chosen near the tip including a minor area on the trapped bead. The position of the ROI is corrected in every image such that the location is constant relative to the centroid of the trapped bead (red dot) which becomes displaced during pulling or pushing (see Movie 5). This ensures that the same region of the tether is quantified in all images. (B) Quantification is performed by thresholding the image with the background intensity plus the standard deviation of the noise as the threshold. Pixels having intensity levels higher or lower than the threshold are given a binary value '1' or '0', respectively. Element by element multiplication of the binary matrix with the raw image followed by summation of all pixels gives the total intensity.

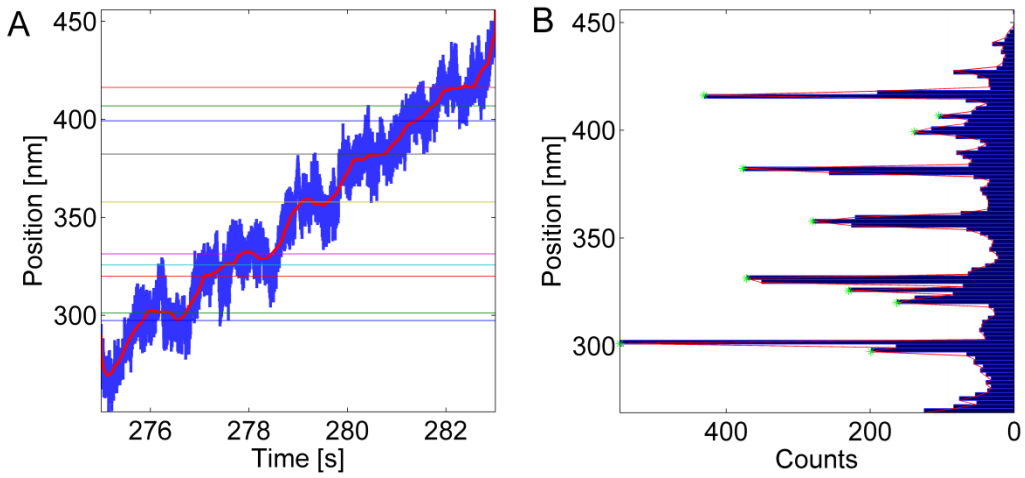

Figure S12 | Evidence of stepwise pulling indicating motor activity in the force transduction mechanism. (A) Time trace showing an example of stepwise behavior. The position of the trapped bead moves in discrete steps towards the cell (cell pulls on the bead). Red line is a running average. Horizontal lines indicate possible steps. (B) Histograms of the positions recorded in (A) to visualize possible steps.

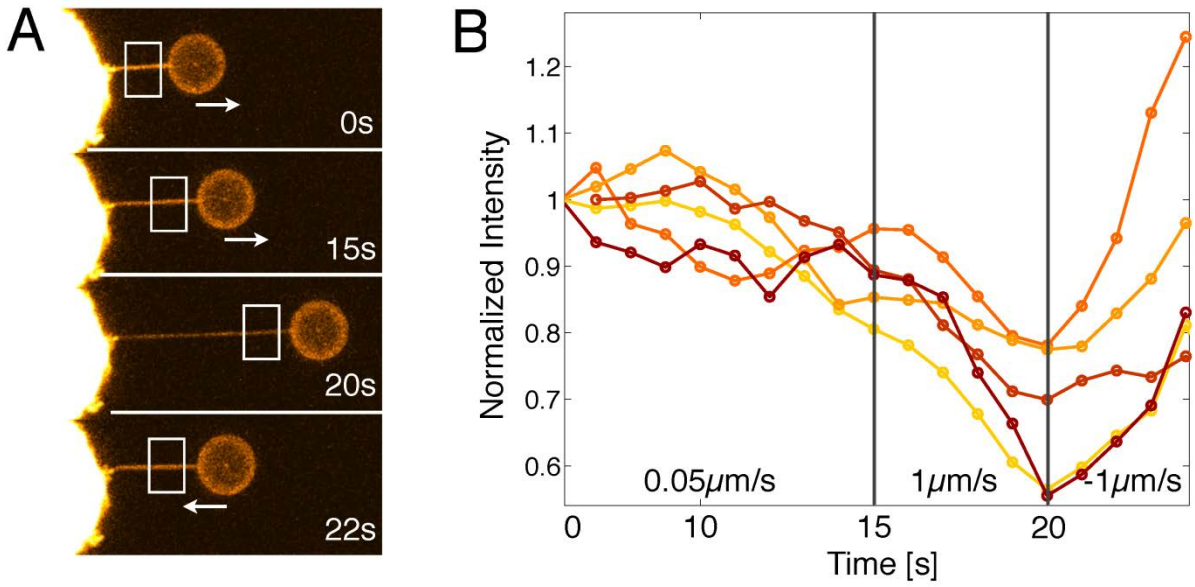

Figure S13 | Filopodia membrane tube is under lateral tension. (A) Rapid elongation and retraction (10 µm) of a calcein AM labeled membrane tube reveals a velocity dependent calcein

intensity. (B) Quantification of the fluorescent intensity versus time. The five different curves represent measurements performed on different filopodial tethers.

1. **Brochard-Wyart F, Borghi N, Cuvelier D, & Nassoy P (2006) Hydrodynamic narrowing of tubes extruded from cells. *Proceedings of the National Academy of Sciences of the United States of America* 103(20):7660-7663.**
2. **Daniels DR & Turner MS (2013) Islands of conformational stability for filopodia. *PloS one* 8(3):e59010.**
3. **Pronk S, Geissler PL, & Fletcher DA (2008) Limits of filopodium stability. *Physical review letters* 100(25).**
4. **Derenyi I, Julicher F, & Prost J (2002) Formation and interaction of membrane tubes. *Physical review letters* 88(23).**
5. **Tirado M & Torre J (1979) Translational friction coefficients of rigid, symmetric top macromolecules. Application to circular cylinders. *J Chem Phys* 71:2581.**
6. **Saffman PG & Delbruck M (1975) Brownian motion in biological membranes. *Proceedings of the National Academy of Sciences of the United States of America* 72(8):3111-3113.**
7. **Tirado M, Martínez C, & Torre J (1984) Comparison of theories for the translational and rotational diffusion coefficients of rod like macromolecules. Application to short DNA fragments. *J. Chem Phys* 81:2047.**
8. **Erb E, Tangemann K, Bohrmann B, Muller B, & Engel J (1997) Integrin alphaIIbeta3 Reconstituted into Lipid Bilayers Is Nonclustered in Its Activated State but Clusters after Fibrinogen Binding. *Biochem* 36:7395-7402.**
9. **Rasband, W.S., ImageJ, U. S. National Institutes of Health, Bethesda, Maryland, USA, http://imagej.nih.gov/ij/, 1997-2014.**
10. **Matlab and Image Processing Toolbox Release 2012b, The MathWorks, Inc., Natick, Massachusetts, United States.**
11. **Hansen PM, Tolic-Norrelykke IM, Flyvbjerg H, & Berg-Sorensen K (2006) tweezercalib 2.1: Faster version of MatLab package for precise calibration of optical tweezers. *Comput Phys Commun* 175(8):572-573.**
12. **Burkel BM, von Dassow G, & Bement WM (2007) Versatile fluorescent probes for actin filaments based on the actin-binding domain of Utrophin. *Cell motility and the cytoskeleton* 64(11):822-832.**
13. **Riedl J*, et al.* (2008) Lifeact: a versatile marker to visualize F-actin. *Nature methods* 5(7):605-607.**